Peer-reviewed version available at *Nanomaterials* **2018**, *8*, 907; doi:10.3390/nano8110907

Article

Title Magnetic Alginate / Chitosan Nanoparticles for Targeted Delivery of Curcumin into Human Breast Cancer Cells

Wenxing Song [1], Xing Su [2], David A. Gregory [1], Wei Li [3], Zhiqiang Cai [4], Xiubo Zhao [1,4,*]

[1]Department of Chemical and Biological Engineering, University of Sheffield, Sheffield S1 3JD, UK
[2]Department of Materials Science and Engineering, University of Sheffield, Sheffield S1 3JD, UK
[3]Department of Electronic and Electrical Engineering, University of Sheffield, Sheffield S3 7HQ, UK
[4]School of Pharmaceutical Engineering and Life Science, Changzhou University, Changzhou 213164, China

* Correspondence: Xiubo Zhao, email: xiubo.zhao@sheffield.ac.uk; Tel: +44 114 222 8256

Abstract: Curcumin is a promising anti-cancer drug but its applications in cancer therapy are limited due to its poor solubility, short half-life and low bioavailability. In this study, curcumin loaded magnetic alginate / chitosan nanoparticles were fabricated to improve the bioavailability, uptake efficiency and cytotoxicity of curcumin to MDA-MB-231 breast cancer cells. Alginate and chitosan were deposited on Fe_3O_4 magnetic nanoparticles based on their electrostatic properties. The sizes of the nanoparticles (120-200 nm) were within the optimum range for drug delivery. Sustained curcumin release was obtained use the nanoparticles with the ability to control the curcumin release rate by altering the number of chitosan and alginate layers. Confocal fluorescence microscopy results showed that targeted delivery of curcumin with the aid of magnetic field were achieved. The FACS assay indicated that MDA-MB-231 cells treated with curcumin loaded nanoparticles had a 3-6 folds uptake efficiency to those treated with free curcumin. MTT assay indicated that the curcumin loaded nanoparticles exhibited significantly higher cytotoxicity toward MDA-MB-231 cells than toward HDF cells. The sustained release profiles, enhanced uptake efficiency and cytotoxicity to cancer cells as well as the targeting potential make MACPs a promising candidate for cancer therapy.

Keywords: Alginate; Chitosan; Layer-by-layer; Magnetic nanoparticles; Drug delivery; Cancer; Curcumin

Abbreviations: CUR: curcumin; CHI: chitosan; MNPs: magnetic nanoparticles; MAPs: Magnetic alginate nanoparticles; MACPs: magnetic alginate / CHI layer-by-layer nanoparticles; CMACPs: Curcumin loaded magnetic alginate / chitosan layer-by-layer nanoparticles; CMACPs 1 & 4: Curcumin loaded magnetic alginate / chitosan layer-by-layer nanoparticles with 1 and 4 layers of CHI/SA coating

1. Introduction

Curcumin (CUR) is a yellow, hydrophobic, polyphenolic compound of turmeric that is extracted from the rhizomes of *Curcuma longa,* which is widely cultivated in Asian countries such as India and China and has been historically used as a spice [1,2]. CUR is considered

Peer-reviewed version available at Nanomaterials 2018, 8, 907; doi:10.3390/nano8110907

'Generally Recognized as Safe (GRAS)' by the Food and Drug Administration (FDA) [1] and has been widely employed in medicine attributed to its anti-oxidant [3-5], anti-inflammatory [6-8], wound-healing [9,10] and anti-bacterial [11,12] activities. Recent research has demonstrated that CUR has the ability to inhibit the carcinogenesis in various cell lines including breast, colon and gastric cancer cells, resulting in increased interest as a promising drug for cancer therapy [13-16]. However, CUR exhibits poor solubility in aqueous solutions, limiting its applications in cancer therapy [17-19].

It has been reported that after the oral administration of 2 g/kg of CUR to human, an extremely low serum concentration (0.006 ± 0.005 μg/ml) of CUR was observed after 1 h [20]. As a result, the bioavailability and anti-cancer efficiency of CUR is limited by its low solubility [17-19]. In order to improve the anti-cancer efficiency of CUR, various nanocarriers have been used, including lipid based nanoparticles [21-25], polymer nanoparticles [26-32] and inorganic nanoparticles [33]. The main advantages of the CUR loaded nanocarriers are their small size and large surface area which results in the ability of these carriers to pass through the cell membranes with enhanced uptake efficiency, delivering the cargos into the cells [1,30]. Research has increasingly focused on the fabrication of biopolymer nanoparticles for CUR delivery due to advantages of low cytotoxicity, biocompatibility, biodegradability and environmental-friendly [30]. Two of the most commonly used biopolymers in medical applications are alginate and chitosan (CHI). Alginate is an anionic polysaccharide composed of (1-4)-linked β - D-mannuronate (M) and α -L-guluronate (G) residues and CHI is a cationic polysaccharide composed of N-acetyl-D-glucosamine and D glucosamine [34,35]. CHI is positively charged in water at acidic and neutral pH due to the protonation of amino groups from CHI chains [36]. Both alginate and chitosan (CHI) are naturally obtained biopolymers that possess desirable properties such as biocompatibility, biodegradability and are not toxic [35]. Moreover, alginate based nanoparticles can be fabricated by a simple process of Ca^{2+} cross-linking or altering of pH [37]. CHI based nanoparticles can be prepared by providing polyanion of tripolyphosphate (TPP) without introducing harsh cross-linking agent or organic solvents [38]. Electrostatic interactions between positive CHI chains and negative drugs such as CUR enables the retention of the

Peer-reviewed version available at Nanomaterials 2018, 8, 907; doi:10.3390/nano8110907

drug in CHI based nanoparticles providing a prolonged drug release profile [39]. These advantages of alginate and CHI make them promising candidates as nanocarriers for drug delivery [35]. In fact, various alginate or CHI based nanoparticles have been developed for the delivery of CUR [32,40-43]. For example, Anitha *et al*. [40] prepared CUR loaded dextran sulphate–chitosan nanoparticles and reported that a controlled and pH dependent CUR release over a period of one week was achieved. Maghsoudi *et al.* [42] prepared CUR loaded alginate nanoparticles and reported that the CUR loaded nanoparticles exhibited enhanced solubility in aqueous solutions comparing with free CUR.

Exploiting the electrostatic properties of alginate and CHI, a layer-by-layer coating method can be employed to prepare multilayer alginate / CHI polyelectrolyte nanoparticles, this method allows simple engineering of desired surface features for specific applications [44]. By altering the amount of layers deposited it is possible to control the drug release rate [45-47]. In addition, the use of a noncovalent route for multilayer formation provides a low-cost simple fabrication method [48]. Due to these promising advantages of the layer-by-layer method, it has been widely used to fabricate nanoparticles for drug delivery [44-47,49]. Apart from engineering the size and surface properties of nanocarriers, incorporation of magnetic nanoparticles (MNPs) enables the targeted delivery of the drug carriers to tumour sites with the help of an external magnetic field [50]. Targeted delivery by MNPs has been reported as a promising strategy for cancer therapy, which possesses the advantages including visualize the targeting process, rapid targeting and accumulation of drug carriers at the tumour sites by magnetic forces, the MNPs can be heated in a magnetic field to promote the drug release and avoiding complex chemical modifications of targeting ligands on the surface of nanoparticles [50]. The toxicity of MNPs have been reported very low and can be well tolerated in the human body [51]. The small size and large surface area of MNPs make them suitable for polyelectrolyte layer-by-layer deposition. Therefore, deposition of alginate / CHI multilayers onto MNPs will enable targeted delivery and controlled released of drugs. In this paper, magnetic alginate / CHI layer-by-layer nanoparticles (MACPs) were fabricated for the delivery of CUR into MDA-MB-231 breast cancer cells and HDF cells.

Peer-reviewed version available at Nanomaterials 2018, 8, 907; doi:10.3390/nano8110907

2. Materials and Methods

2.1. Materials

Curcumin (C8069) was purchased from LKT Laboratories. Paraformaldehyde (sc-253236A) was purchased from Chem Cruz®. Sodium alginate (w201502), Na_2HPO_4 (S7907), NaH_2PO_4 (S8282), ammonium hydroxide (221228), $Ca(OH)_2$ (21181) and DMSO (Dimethyl sulfoxide, D5879) were purchased from SIGMA-ALDRICH. RPMI (Roswell Park Memorial Institute) 1640 Medium (BE 12-167F), PBS (Dulbecco's Phosphate Buffered Saline, BE17-512F), Penicillin 5,000 U/ml-Streptomycin 5,000 U/ml (DE17-603E), L-Glutamine (17-605F) were purchased from Lonza®. Chitosan (349051000), Iron (II) chloride tetrahydrate (44939), Iron (III) chloride hexahydrate (44944), $NaHCO_3$ (A17005), Alexa Fluor® 568 phalloidin (A12380), MTT (M6494) assay, FBS (Fetal Bovine Serum, 10500064) and DAPI (4′, 6-Diamidino-2-phenylindole dihydrochloride, D1306) were purchased from Thermo Fisher Scientific. MDA-MB-231 cells (Human Caucasian Breast Adenocarcinoma cells) were purchased from ECACC.

2.2. Preparation of nanoparticles

2.2.1. Preparation of Fe_3O_4 magnetic nanoparticles

Fe_3O_4 MNPs were prepared by the coprecipitation method described previously in Song *et al*. [28]. 4 g Iron (III) chloride hexahydrate and 4.5 g Iron (II) chloride tetrahydrate were each dissolved in 150 ml DI water and degassed with nitrogen for 30 min to replace any oxygen in the solutions. The solutions were then mixed in a 500 ml round-bottom flask and 15 ml of ammonium hydroxide was added under vigorous stirring in a nitrogen atmosphere at room temperature. The solution was then vigorously stirred for 2 h and the formed MNPs were collected with strong Neodymium magnets and washed several times with DI water until neutral pH was registered. Finally, the magnetic nanoparticles were dried over night at room temperature and stored for future usage.

2.2.2. Preparation of magnetic alginate nanoparticles

Magnetic alginate nanoparticles (MAPs) were prepared based on the procedure described by Liu *et al*. [52] 20 ml of ethanol and 10 ml of DI water was mixed into a beaker and 0.25 g of MNPs were suspended in the prepared mixture. Next, 40 ml of sodium alginate (SA) solution (20 mg/ml) was added to the beaker upon which the mixture was sonicated for 10 min to allow full homogenous dispersion of MNPs in the suspension. The resultant mixture was vigorously stirred for 30 min at room temperature. Subsequently, 128 ml of $Ca(OH)_2$ solution (0.74 mg/ml) was added into the suspension and stirred for 1 h before 16 ml of $NaHCO_3$ solution (10 mg/ml) was added. The suspension was then stirred for a further 12 h at room temperature and the resulting MAPs were collected with strong Neodymium magnets, washing thoroughly with ethanol and water to remove excess salts. Finally, purified MAPs were suspended in DI water before used in the layer-by-layer process.

2.2.3. Preparation of magnetic alginate / chitosan layer-by-layer nanoparticles

The preparation of magnetic alginate / chitosan layer-by-layer nanoparticles (MACPs) was based on the layer-by-layer self-assembly of SA and CHI on MAPs. Chitosan solution (10 mg/ml) was prepared in 1% (v/v) acetic acid aqueous solution. The first layer was deposited by adding 1 g of MAPs into 100 ml of the chitosan solution under vigorous stirring for 20 min at room temperature. The resultant MA / CHI particles were collected with a Neodymium magnet and the excess CHI was removed by washing the particles several times with DI water. The next SA layer was deposited by adding the previously prepared particles into 100 ml of SA solution (10 mg/ml) under vigorous stirring for 20 min thus forming MA / CHI / SA particles. For each layer the previously described purification process was used. Particles with more layers were fabricated by alternatively coating positively charged CHI and negatively charged SA on MACPs until the desired number of layers was reached.

Peer-reviewed version available at Nanomaterials 2018, 8, 907; doi:10.3390/nano8110907

2.3. Curcumin loaded magnetic alginate / chitosan layer-by-layer nanoparticles

Firstly, 20 ml of CUR solution (7.5 mg/ml in DMSO) was added into 30 ml of DI water to prepare the CUR mixture (3 mg/ml). Then 30 mg of MACPs were added into 20 ml of the CUR mixture and stirred for 24 h. The resultant CUR loaded magnetic alginate / chitosan layer-by-layer nanoparticles (CMACPs) were collected with a Neodymium magnet and washed three times with DI water. The supernatants were collected and analysed with a UV-Vis spectrometry (JENWAY 6715, Bibby Scientific, UK) to determine the concentration of residual CUR. The CMACPs were dispersed in 5 ml of DI water and the concentration of these particles was determined by weighing dried particles from 1 ml solution. Encapsulation and loading efficiencies were determined by Eq.(1), where $EE\%$ is the Encapulation Efficiency, mP_{CUR} is the amount of CUR encapsulated in particles, m_{intCUR} is the amount of CUR initially added. In Eq.(2), $LE\%$ is the Loading Efficiency and N_P is the total amount of CUR loaded particles:

$$EE\%_{(w/w\%)} = \frac{mP_{CUR}}{m_{\text{int}CUR}} \times 100\% \quad (1)$$

$$LE\%_{(w/w\%)} = \frac{mP_{CUR}}{N_P} \times 100\% \quad (2)$$

2.4. Release of CUR from CMACPs

5 mg of CMACPs were suspended in 5 ml PBS buffer (pH 7.4) in vials and incubated at 37 °C under constant shaking (200 rpm). The particles were collected with strong Neodymium magnets at pre-determined time points and the supernatants were carefully removed before re-disperseing the particles in 5 ml fresh PBS. The CUR concentrations of the supernatants were analysed using UV-Vis-spectrometry and the percentage of cumulative CUR release was plotted as a function of incubation time.

2.5. Particle characterization

2.5.1. Nano particle tracking and zeta potential analysis

MACPs and CMACPs were dispersed in sodium phosphate solution (10 mM, pH 7) and injected into the scattering cell of an NTA (Nanosight LM10, UK) where their motion was analysed and average size was calculated. The zeta potential measurement of particles was carried out by a Dynamic light scattering analyser (DLS, NanoBrook 90 plus Pals Particle size Analyzer, Brookhaven Instrument, NY, USA). Particles were washed several times and dispersed in DI water (pH 6.5-7.5) or 10 mM sodium phosphate buffer (pH 7) prior to zeta potential measurements.

2.5.2. Fourier transform infrared spectroscopy

Fourier transform infrared spectroscopy (FTIR) analysis was conducted with the Spectrum 100 spectrophotometer (PerkinElmer, USA). Particles were washed three times with DI water and dried in an oven at 60 °C for 24 hours before being placed on the diamond attenuated total reflectance (ATR) accessory and compressed. The wavenumber region was set from 4000 to 600 cm^{-1} with a resolution of 1 cm^{-1}. The spectral processing was conducted with the software (IRPal 10) provided within the FTIR instrument.

2.5.3. Atomic Force Microscopy analysis

The aggregation size and morphology of particles was characterised using Atomic Force Microscopy (AFM, Dimension Icon with ScanAsyst, Bruker Corporation, U.S.A). Particle suspensions were dropped on mica substrates and air dried before being placed on the sample stage. AFM measurements were conducted using SCANASYST-AIR tips and data was analysed with NanoScope Analysis 1.5 software.

Peer-reviewed version available at Nanomaterials 2018, 8, 907; doi:10.3390/nano8110907

2.5.4. Transmission electron microscopy analysis

MACPs or CMACPs were dispersed in DI water and dropped onto copper TEM grids and incubated at room temperature for 30 s. Excess solution on grids was then removed with filter paper, by gently dapping the edge and allowing excess liquid to be absorbed prior to transmission electron microscope (TEM) imaging (Tecnai G2 Spirit, FEI, USA). An acceleration voltage of 80 kV was used and images were recorded using a Gatan Orius SC1000B bottom mounted digital camera and analysed in Gatan Digital Micrograph software (version 3.9.1).

2.6. Cellular uptake assays

CUR medium solutions were prepared by adding CUR dissolved in DMSO (50 mg/ml) dropwise into media to obtain different final CUR concentrations (0.5, 1.5, 5, 15, 30 μg/ml). CMACPs were dispersed in media to reach the final CUR concentrations equivalent to those of CUR medium solutions. MDA-MB-231 and HDF cells were seeded in 6 well plates at a density of 3×10^5 cells per well and incubated overnight at 37 °C and 5% CO_2. Then the mediums were removed and replaced with 2 ml CUR medium solutions or CMACPs medium solutions and incubated for a further 24 h. After this, the cells were harvested with trypsin and washed twice with PBS to remove any free CUR or CMACPs. The resultant cells were collected and analysed with the BD™ LSR II flow cytometer (BD Biosciences, USA) to investigate the cells CUR uptake.

2.7. Magnetically targeted delivery assay

MDA-MB-231 cells were seeded in glass bottom dishes (Nunc™, Thermo Scientific, diameter 35 mm) at a density of 3×10^5 cells per dish and incubated for overnight to allow the attachment. Free CUR and CMACPs were added into cell cultures to reach a final CUR concentration of 5 μg/ml and incubated for 4 h. Magnetically targeted delivery was conducted by initially placing a Neodymium magnet under the dish for the first 15 min during incubation. Cells were then washed twice with PBS buffer and fixed with 4 %

Peer-reviewed version available at Nanomaterials 2018, 8, 907; doi:10.3390/nano8110907

paraformaldehyde. The fixed cells were stained with Alexa Fluor 568 Phalloidin and DAPI for 1 h. The confocal fluorescence images of cellular uptake of CUR were observed with an Inverted Zeiss LSM 510 NLO microscope (Zeiss, Germany) and analysed with LSM Image Browser software version 4.2.0.121.

2.8. *In vitro* cytotoxicity assay

The cytotoxicity of free CUR, MACPs, and CMACPs against MDA-MB-231 and HDF cells was investigated using the MTT assay. MDA-MB-231 or HDF cells were seeded into 96-well plates at a density of 5×10^3 cells per well and incubated overnight at 37 °C and 5% CO_2. The media were then removed and replaced with CUR medium solution, MACPs or CMACPs dispersions (CUR content in the particles is equivalent to the dosage of free CUR) to reach the final CUR concentration of 0.5, 1.5, 5, 15, 30 μg/ml. After 48 h of incubation, 50 μl of 3 mg/ml MTT was added to each well and incubated at 37 °C for 3 hours followed by removing the supernatants and adding 200 μl DMSO. A plate reader (FLUOstar galaxy, BMG LABTECH, Germany) was used to measure the absorbance of each well including control wells containing only medium at 570 nm. The relative cell viability was determined by comparing the absorbance with control wells.

3. Results and discussion

3.1. Characterization of magnetic alginate / chitosan layer-by-layer nanoparticles and curcumin loaded magnetic alginate / chitosan nanoparticles

3.1.1. Zeta potential, size and FTIR spectra

As shown in Scheme, magnetic alginate particles (MAPs) were prepared via the self-assembly of alginate on the surface of MNPs in Ca^{2+} solution (Stage 1). Following this the formation of MACPs (Stage 2) was achieved by coating MAPs with CHI. Stage 3: Particles with 1 layer of SA and CHI were then coated with SA again on particles. Stage 2 and 3 were then repeated consecutively for the desired amount of layers.

Preprints (www.preprints.org) | NOT PEER-REVIEWED | Posted: 28 September 2018 doi:10.20944/preprints201809.0558.v1

Peer-reviewed version available at Nanomaterials 2018, 8, 907; doi:10.3390/nano8110907

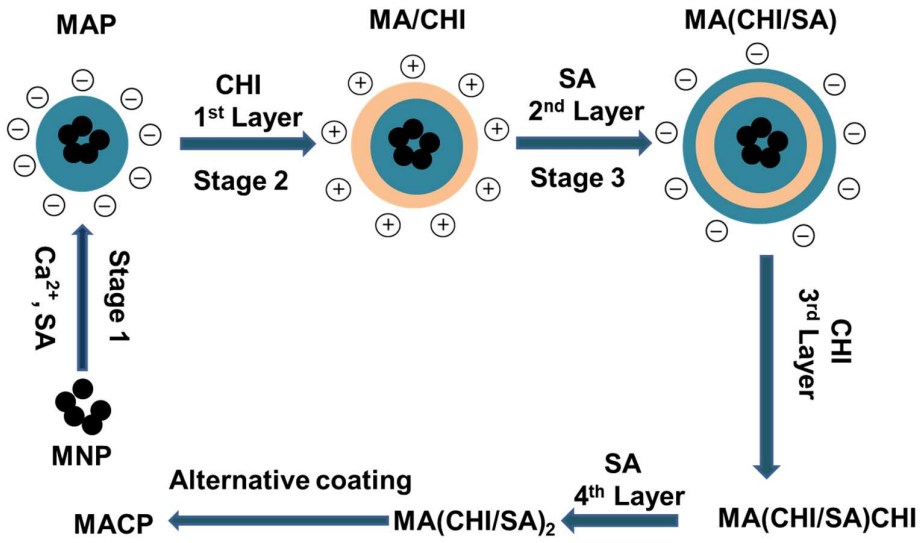

Scheme 1. Schematic illustration for the preparation of MAPs and MACPs. MAPs were fabricated by coating cross-linked alginate on MNPs using Ca^{2+} as the cross-linker. MACPs were prepared by alternatively depositing CHI and SA on MAPs based on the electrostatic interaction between the two biopolymers. The alternative coating was repeated until MACPs with desired number of layers were obtained (Stage 2 and 3).

MAPs and MACPs with different number of layers were dispersed in DI water (pH was adjusted to 7 using HCl and NaOH) or sodium phosphate solution (pH 7) and their zeta potential was analysed using DLS. As shown in Fig. 1a, the zeta potential of MAPs in water was -21.4 mV which was similar to the results of Ca^{2+} crosslinked alginate particles reported in previous literature [53,54]. The zeta potential of free SA in water has been reported as -50 mV [55]. The reason for the increased zeta potential of MAPs is due to crosslinking with Ca^{2+}. The carboxyl groups contribute to the anionic charge of the alginate polymer [56]. Upon gelation, the negatively charged carboxyl groups from the G blocks in the alginate chains interact with Ca^{2+} ions and form an 'egg-box'-like structure, reducing the density of free carboxyl groups as well as the anionic charges [56]. Therefore, an increase of zeta potential was observed for MAPs. After deposition of the first layer (CHI), zeta potential of particles become positive (+19.2 mV) followed by a reduction to -44.8 mV after the negatively charged alginate polymer was coated as the second layer. Positive charges ranging from +12.1 to +19.2 mV were observed when CHI was coated as the outermost layer and negative charges

Peer-reviewed version available at Nanomaterials 2018, 8, 907; doi:10.3390/nano8110907

ranging from -43 to -48.5 mV were associated with alginate coatings as the outermost layer. An oscillation of zeta potential was observed with the alternative deposition of SA and CHI, indicating the successful coating of negative alginate and positive chitosan polymers.

The zeta potential of particles in sodium phosphate solution (10 mM) is also shown in Fig. 1a and exhibited similar oscillation behaviour. However, negative surface charges were observed for MACPs (layer number: 1, 3, 5, 7, 9) with CHI outermost layer. This phenomenon is due to the adsorption of the phosphate anion onto the surface of the chitosan polymers. Phosphates, as small multivalent anions, tend to interact or complex with cationic amino groups and adsorbed on CHI surfaces via electrostatic interactions [38]. Therefore, the phosphate anions adsorbed on CHI layers increased the negative charges on the particles. Similar phenomena have been reported previously: for example, Swain *et al.* [57] analysed the zeta potential of CHI in both 1 and 10 mM NaCl and found that the zeta potential value decreased as the ionic strength of NaCl increased. The authors suggested the reduced surface charges was attributed to the adsorption of anions on the surface of CHI polymers [57]. Further to this, Acevedo *et al*. [58] analysed the zeta potential of CHI (5 mg/ml) in water and NaCl solution (0.2 M) and reported that the zeta potential value was +72 mV in water and +33 mV in NaCl solution. It was suggested that this reduced absolute value behaviour was governed by a compression of the electrical double layer due to the electrostatic interactions with Cl^- in the solvent [58]. As shown in Fig. 1a, The zeta potential of MACPs with alginate as the outermost layer analysed in phosphate solution exhibited similar values as they were in water, which is in agreement with previously reported data [55]. On the other hand, MAPs exhibited an increased negative zeta potential value in phosphate solution (-36 mV) compared to that in water (-21.4 mV). This is due to reaction between Ca^{2+} and phosphate ions to form insoluble calcium phosphate which leads to the loss of Ca^{2+} and the increased density of free carboxyl groups thus resulting in an overall increased negative charges. The zeta potential behaviour of drug carriers can be utilized to control the drug loading and release processes. For example, cationic drug carriers such as CHI nanoparticles can be used to improve the loading of anionic drug molecules and prolong their release time based on the electrostatic interactions between positive CHI and negative drug molecules

[39]. In the case of MACPs, different numbers of polymer layers with different zeta potentials can potentially be used to improve drug loading.

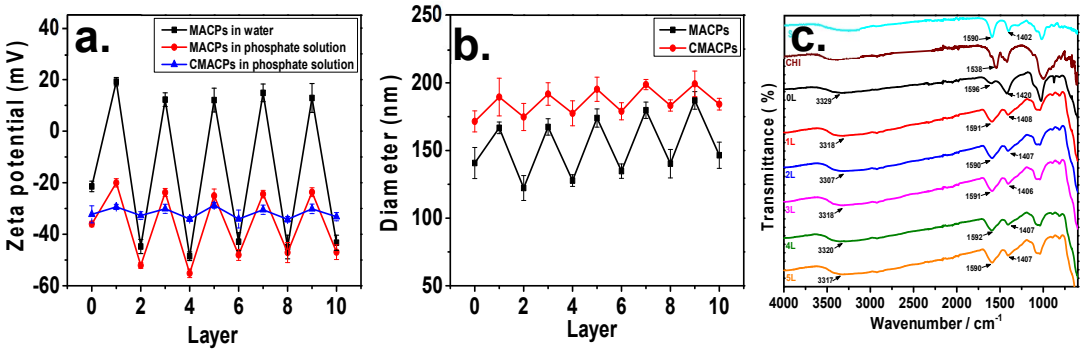

Fig. 1. Zeta potential (a) and average diameter (b) of MACPs and CMACPs as a function of the number of coated layers. Zeta potential of particles was analysed in water (pH 7) and phosphate solution (10 mM, pH 7). Particle size was analysed in phosphate solution. Oscillations of zeta potential and average diameter were observed with the alternate coating of SA and CHI. (c) FTIR spectra of MAPs and MACPs with the number of deposited polymer layers from 1 to 5. The results are shown in mean ± SD, n ≥ 3.

The average diameter of MACPs was analysed by NTA as shown in Fig. 1b, where the diameter of MACPs was seen to be 141 nm and increased to 167 nm after the coating of the first CHI layer. The size of particles increased gradually as the coating of SA / CHI bilayers and reached 187 nm for 9 layers. The growth in particle size is attributed to the deposition of SA and CHI polymers. The differences in size depending on the outermost polymers of MACPs were also observed. For example, after coating with the second layer (SA), the average diameter of MACPs decreased from 167 (3 layers) to 128 nm (4 layers) and then increased to 174 nm after the deposition of CHI as the fifth polymer layer. This leaves a mean size difference of ~40 nm between CHI and SA and is most likely due to the different surface charges of the particles. For MACPs with CHI as the outermost layers, the zeta potential ranged from -20 to -25.1 mV in phosphate buffer solutions while the zeta potential of alginate outermost layer ranged from -47 to -55.2 mV. Particles with absolute zeta potential values higher than 30 mV can be considered stable in solution [59]. Therefore,

Peer-reviewed version available at Nanomaterials 2018, 8, 907; doi:10.3390/nano8110907

MACPs with alginate outermost layers were very stable in solution due to their sufficient surface charges. On the other hand, particles with CHI as the outermost layers were more likely to aggregate in the solution, thus form the larger particle size.

The zeta potential of CMACPs in sodium phosphate solution at pH 7 is also shown in Fig. 1a. A significant change in surface charge was observed for particles after CUR loading. The zeta potential of free CUR sodium phosphate solution was -31.1 mV. In contrast, the zeta potentials of MAPs and MACPs with the outermost layer of alginate (layer number: 0, 2, 4, 6, 8, 10) was within the range from -36 to -55.5 mV (Fig. 1a) while the zeta potentials of the particles with CHI outermost layer (layer number: 1, 3, 5, 7, 9) were around -20 mV. After the CUR loading process, the zeta potentials of CMACPs were found between -28.7 – -34.2 mV suggesting the CUR was encapsulated in or adsorbed onto the particles, reducing the difference of the zeta potentials between MACPs with alginate and CHI outermost layers. Increased particle sizes were observed for CMACPs between 172–199 nm (Fig. 1b) compared to MACPs 122–187nm which is resulted from the loading of CUR. For CMACPs with the same outermost polymer (SA or CHI), the average diameter of particles increased as the numbers of layer increased due to the fact that larger polymer matrixes provided larger space for CUR molecules to be encapsulated. Slightly larger particle size was observed for CMACPs with the outermost polymer of CHI compared to those with SA as the outermost layer. This is because CMACPs with SA outermost layers exhibited a higher absolute value of zeta potential than those with CHI. They possessed a greater electrostatic repulsion therefore maintained smaller aggregation sizes. It is worth to note that the size of CMACPs were also within the range of 50-200 nm. For the efficient delivery of drug to the cancer sites, the optimum size range of drug carriers is generally accepted to be about 50-200 nm [60]. Particles with size less than 50 nm will easily extravasate through the discontinuous endothelium of live, spleen and bone marrow therefore are less likely to accumulated at the desired sites. On the other hand, particle with diameter larger than 200 nm may not pass through the porous vasculature to reach the tumour site and will be eliminated more easily by the immune system [60]. Therefore, CMACPs are within the optimum size range for the delivery of drugs to the tumour sites.

Peer-reviewed version available at Nanomaterials 2018, 8, 907; doi:10.3390/nano8110907

The chemical compositions and interactions between different polymer layers were analysed by FTIR as shown in **Error! Reference source not found.**. For SA, the peaks at 1590 cm^{-1} and 1402 cm^{-1} were characteristic for the asymmetric stretching and symmetric stretching of -COOH groups respectively [61,62].In MAPs and MACPs with the number of layers (1, 2, 3, 4 and 5, these two peaks moved toward higher wavenumbers, which were evidences of the formation of Ca^{2+}-alginate ionic cross-linking [63]. This is because of the changes in charge density, atom radius and atom weight of the cations [63,64]. For chitosan (CHI), the peak at 1538 cm^{-1} was characteristic of -NH_2 bonds [65]. The presence of chitosan in the MACPs were also confirmed by comparing the curves of MAPs (0 L) and MACPs (1 L - 5 L). First, the broad characteristic adsorption at 3329 cm^{-1} for -OH groups in MAPs shifted to a lower frequency for MACPs (1-5 L), demonstrating the superposition of amine N-H stretching in chitosan and -OH groups of alginate and chitosan [65,66]. The peak at 1596 cm^{-1} in MAPs became broader, and moved to a lower frequency for MACPs, which is attributed to the overlapped -NH_2 stretching from chitosan and -COOH stretching from alginate [67]. These results confirmed that CHI and alginate chains were successfully incorporated into MACPs.

3.1.2. Morphology characterization

In addition to DLS and NTA the size distribution and morphology of MAPs and MACPs were also analysed by AFM and TEM (Fig. 2). As shown in Fig. 2a, particles with diameters around 140 nm were observed and exhibited rough surfaces, which were attributed to the aggregation of small solid MAPs. This finding is in consistent with the MAPs size analysed by NTA. After alternate coating with SA and CHI, the resultant MACPs (Fig. 2b-f) exhibited spherical shapes and smooth surfaces, which further confirmed the successful coating of both polymers. For MACPs, inter-digitation among the adjacent CHI / SA layers were constructed due to the existence of surface charges [68]. Therefore, after the removal of excess polymers, stable films were formed by soft polymers of CHI and SA, which led to the smooth surface of MACPs.

Peer-reviewed version available at Nanomaterials 2018, 8, 907; doi:10.3390/nano8110907

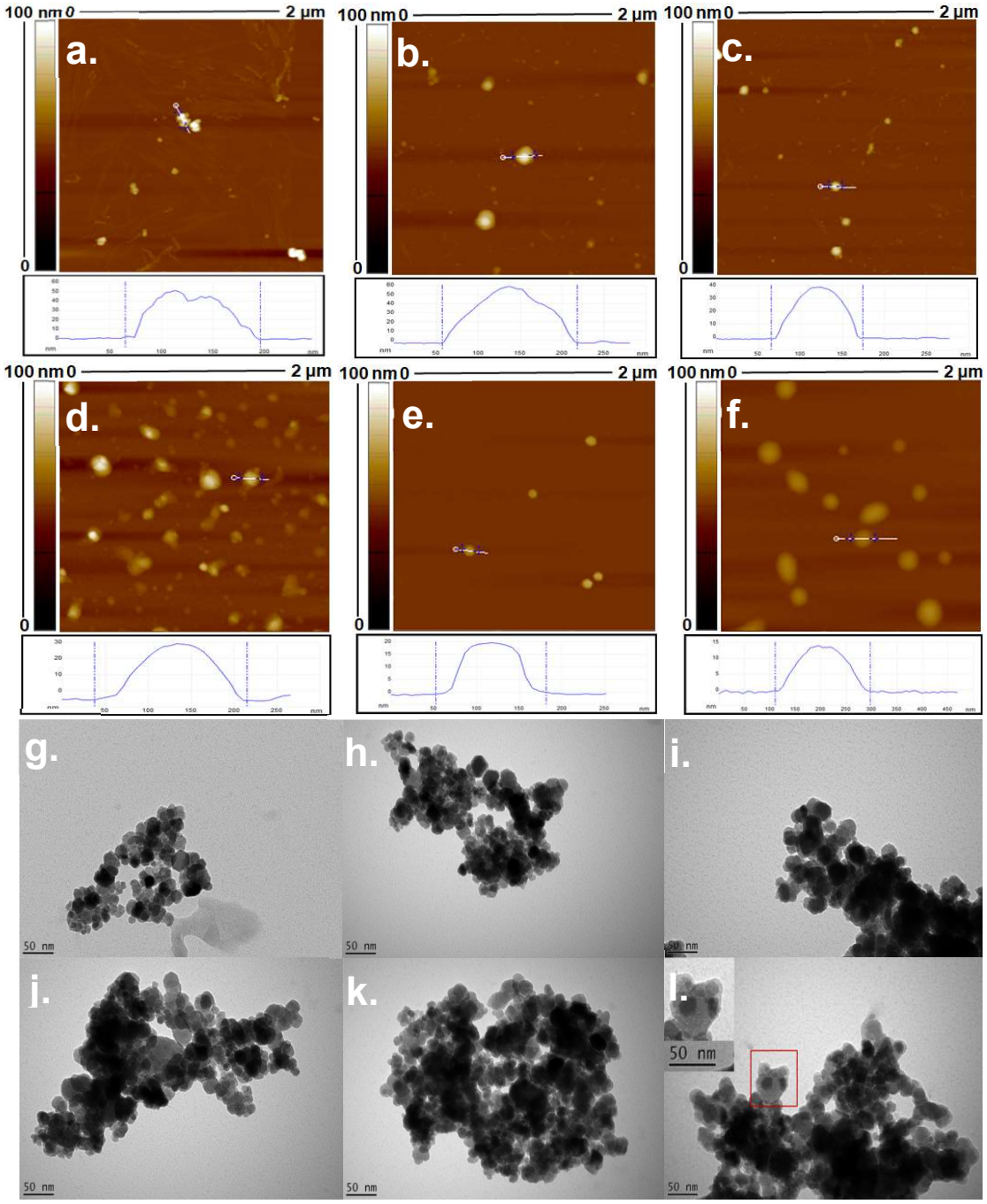

Fig. 2. AFM and TEM images of MAPs (a and g) and MACPs with the layer number of 1 (b and h), 4 (c and i), 5 (d and j), 8 (e and k) and 9 (f and l). Smaller particles were observed for MACPs with SA as the outermost layer.

Moreover, AFM images showed that MACPs with SA as the outermost layer (Fig. 2c&e) exhibited smaller sizes, which is consistent with the NTA measurements and confirmed the

Peer-reviewed version available at Nanomaterials 2018, 8, 907; doi:10.3390/nano8110907

result that MACPs with SA as the outermost layer are more stable due to their lower zeta potential values. Characterisation of MAPs and MACPs via TEM revealed magnetic cores (dark areas) surrounded by polymer shells, which were the chitosan and alginate layers as shown in **Error! Reference source not found.**. The inset in **Error! Reference source not found.** is an enlarged section of the image clearly showing magnetic core particles and the surrounding CHI / SA layers.

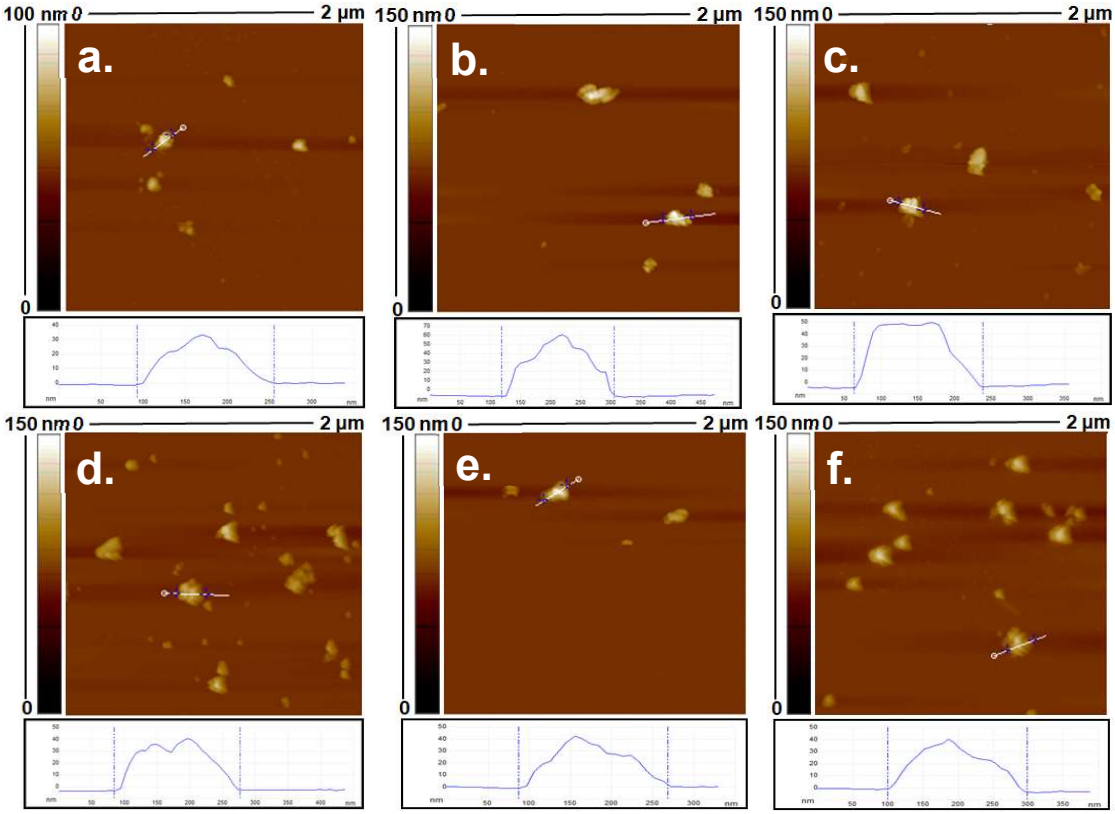

Fig. 3. AFM images of CUR loaded MAPs (a) and CUR loaded MACPs (CMACPs) with the layer number of 1 (b), 4 (c), 5 (d), 8 (e) and 9 (f).

AFM was also used to investigate the morphology of CMACPs. As shown in Fig. 3a, the diameter of CUR loaded MAPs was ~150 nm and increased as the polymer layer increased, reaching a maximum of ~200 nm for 9 layers (Fig. 3f), which is in agreement with the average size analysed by NTA as shown in Fig. 1b. However, rougher surface morphology was observed for CMACPs compared to MACPs as shown in Fig. 2. CUR is known as a highly hydrophobic drug [69-71] and the loading of CUR into MACPs increased the hydrophobicity

Peer-reviewed version available at Nanomaterials 2018, 8, 907; doi:10.3390/nano8110907

of the particles. This meant that the particles rapidly dehydrated during AFM analysis and exhibited rough surfaces, indicating the successful loading of CUR into MACPs.

3.2. Loading and release of curcumin

CUR loaded MACPs were prepared by dispersing MACPs in CUR water / DMSO solution and incubated under stirring for 24 h. The addition of DMSO increases CUR solubility and its permeability into MACPs. The volume ratio of water : DMSO was 3:2, resulting in a homogeneous CUR solution (3 mg/ml) without sedimentation during the 24 h of incubation.[72] Fig. 4a clearly demonstrates that the resultant CMACPs can be collected and washed with Neodymium magnets while CUR itself in the bulk solution was not affected by the magnetic field. Therefore, MACPs can be potentially used targeted delivery of CUR via external magnetic fields.

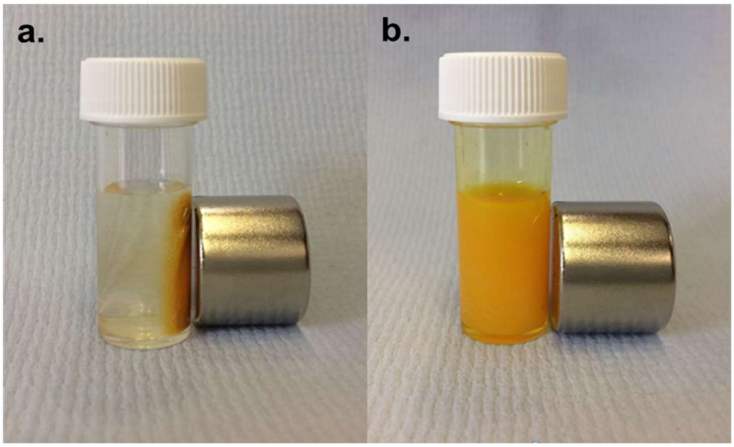

Fig. 4. CMACPs were prepared by suspending MACPs in CUR water / DMSO solution and incubating for 24 h under stirring. The resulting CMACPs can be rapidly collected by a Neodymium magnet (pull force 25 Kg, 25.4 mm Diameter x 30 mm Thick) within 1 min (a). The free CUR in solution on the other hand was not affected by the magnetic force (b).

Encapsulation efficiency results reveal that 49.2% of CUR was loaded into CMAPs and the encapsulation efficiency increased to 67.5% with increasing number of layers of CHI and SA (see Fig. 5a). For particles with the same type of polymer (CHI or SA) on the outermost surface an increased trend of encapsulation efficiency was observed with the increase of the layer number. This phenomenon indicated that increasing the polymer coating layers

Peer-reviewed version available at Nanomaterials 2018, 8, 907; doi:10.3390/nano8110907

allowed more CUR loading, indicating that increased polymer matrix is able to retain more CUR. However, as illustrated in Fig. 5a, a higher encapsulation efficiency of CUR was observed for CMACPs with CHI as the outermost layer (layer number: 1, 3, 5, 7 and 9) compared to that use SA as the outermost layer (layer number: 2, 4, 6, 8, 10). The most feasible explanation for this is that the different surface charges between the particles outermost layers. As illustrated in Fig. 1a, CHI layers exhibited positive surface charges in water while SA layers exhibited relatively high negative surface charges. Therefore, the negatively charged CUR molecules are adsorbed on the surface of CHI layer more readily, facilitating a more efficient and fast encapsulation into polymer matrix. On the other hand, SA layer was negatively charged in water, and thus CUR molecules were less readily to interact with the negatively charged particle surface and enter the polymer matrixes due to the electrostatic repulsion. Moreover, larger amount of CUR molecules were expected have retained on the surface of CHI layer, which also leaded to the higher encapsulation efficiency of CUR in CMACPs with the outermost layer of CHI. Same hypothesis can be used to explain the loading efficiency of CMAPs and CMACPs. As shown in Fig. 5b, a higher loading efficiency of CUR was observed for MACPs with CHI as the outermost layer to those that possessed SA as the outermost layer. Higher loading efficiencies from 54.8% to 64.9% were achieved for CMAPs and CMACPs compared to many previously reported CUR loaded CHI and alginate based particles [26,29,40] that reported the loading efficiencies from 2.7 % to 48 %, suggesting CMAPs and CMACPs possess great potential in loading CUR for drug delivery applications.

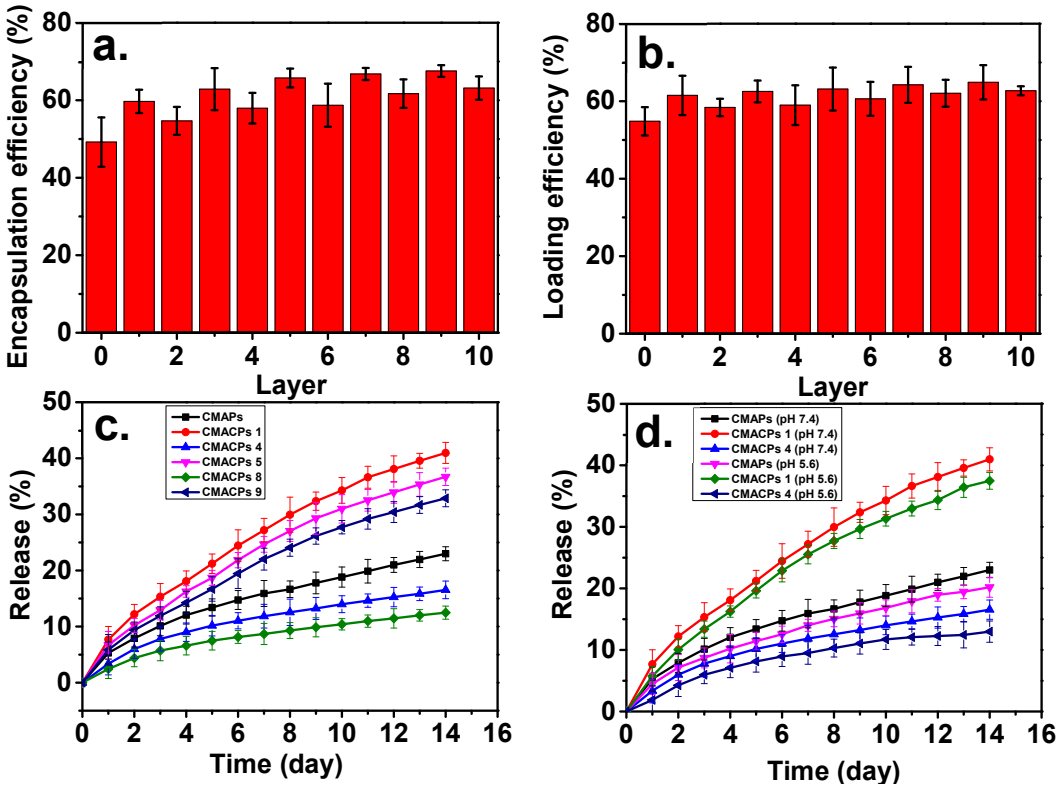

Fig. 5. The drug loading and release profiles of the CMAPs and CMACPs are affected by the type of outermost polymers and the number of layers. Encapsulation efficiency of CMAPs and CMACPs (a). Curcumin loading efficiency into CMAPs and CMACPs (b). Curcumin release profile of CMAPs and CMACPs with different layers (1, 4, 5, 8, 9) of deposited polymers (c). Curcumin release profile of CMAPs and CMACPs (layer number: 1 & 4) in PBS buffer at pH 7.4 and pH 5.6 (d). The results are shown in mean ± SD, n =3.

In order to investigate the release profile of CMAPs and CMACPs, 5 mg of particles were dispersed in 5 ml PBS buffer at pH 7.4 and incubated at 37 °C under shaking (200 rpm) at predetermined time intervals. The particles were collected with strong Neodymium magnets and the CUR concentration in supernatants were analysed to obtain the accumulative CUR release profile. As shown in Fig. 5c, for all particles, CUR was released more rapidly within the first two days and then released slower but at more sustained rates in PBS for up to 2 weeks. The faster release in the first two days is most likely due to the loss of weakly adsorbed CUR molecules on the surface of the particles or in the polymer matrix close to particle surfaces. The sustained CUR release after the first two days was then

Peer-reviewed version available at Nanomaterials 2018, 8, 907; doi:10.3390/nano8110907

dependant on the diffusion of CUR molecules through the polymer matrixes into the bulk PBS solution, thus exhibiting a slower and more sustained release pattern. No significant burst release was observed during the whole release process most likely due to the poor solubility of hydrophobic CUR into aqueous solution[27,73]. During drug release, CMACPs with CHI as the outermost layer exhibited a faster release rate of CUR than CMAPs and CMACPs with SA as the outermost layer (CMACPs 4 and 8). As mentioned previously in section 3.1.1, CHI is positively charged in water but negative in phosphate solution due to the adsorption of negative phosphate ions [38], therefore more negatively charged CUR molecules had been adsorbed on the surface of CHI layers when these particles were dispersed in CUR water / DMSO solution than on alginate layers as illustrated in Fig. 5a&b. When CMACPs with layer numbers of 1, 5 and 9 were dispersed in PBS, phosphate ions competed with CUR molecules for the free amino groups on the CHI chains, which in turn facilitated the loss of CUR molecules from the surface of CHI and the diffusion of CUR from inner polymer matrix (where CUR concentration is higher) to the particle surface. Thus, faster CUR release rates were observed for CMACPs with layer numbers of 1, 5 and 9. On the other hand, CMAPs and CMACPs with layer numbers of 4 and 8, where alginate was deposited as the outermost layer, showed similar negative surface charges in water and phosphate solutions, less CUR molecules were adsorbed during the loading process and thus the drug release rate was not promoted in phosphate solutions. For particles with the same type of polymer, reduced release rates were observed as the number of layers increased (release rate: CMACPs 1 > CMACPs 5 > CMACPs 9, CMAPs > CMACPs 4 > CMACPs 8). By increasing the amount of polymer layers it was more difficult for the innermost CUR to permeate out. This is in agreement with previously reported data [45-47], where Chai *et al.*[45] fabricated doxorubicin loaded poly (lactic-co-glycolic acid) nanoparticles and layer-by-layer coated the particles with CHI and alginate. After comparing the drug release rates of uncoated and polymer coated particles, the authors found that with the CHI / SA coating the initial drug burst release was reduced from 55.1% to 5.8% and overall drug release rate was also reduced. In another example Haidar *et al.*[46] prepared bovine serum albumin loaded liposomes and layer-by-layer coated them with CHI

/ SA. The polymer coated liposomes showed a reduced albumin release rate to the uncoated ones. Further to this Zhou *et al.*[47] developed polyethyleneimine coated PLGA nanoparticles and reported that the drug release rate reduced with increasing layers.

In order to investigate the drug release profile of CMAPs and CMACPs at different pH, CMAPs, CMACPs with 1 and 4 layers were dispersed in PBS with pH 7.4 and pH 5.6. As illustrated in Fig. 5d, the release pattern of CUR from particles at pH 5.6 was similar to those at pH 7.4 but slightly slower. In 14 days, about 23%, 41% and 17% of CUR were released from CMAPs, CMACPs 1 and CMACPs 4 at pH 7.4 respectively while about 20%, 37% and 13% of CUR were released at pH 5.6. The data are in agreement with previously published work by Martins et al.[43] who investigated the release profiles of CUR from N-trimethyl chitosan / alginate complexes at pH 7.4 and pH 1.2 and reported that 80% of CUR was released at pH 7.4 within the first hour while only 22% of CUR was released at pH 1.2. The pH dependent release pattern can be attributed to the altered surface charge and hydrophobicity of polymers at different pH values.

3.3. Cellular uptake assays

3.3.1. CUR uptake assay by flow cytometry

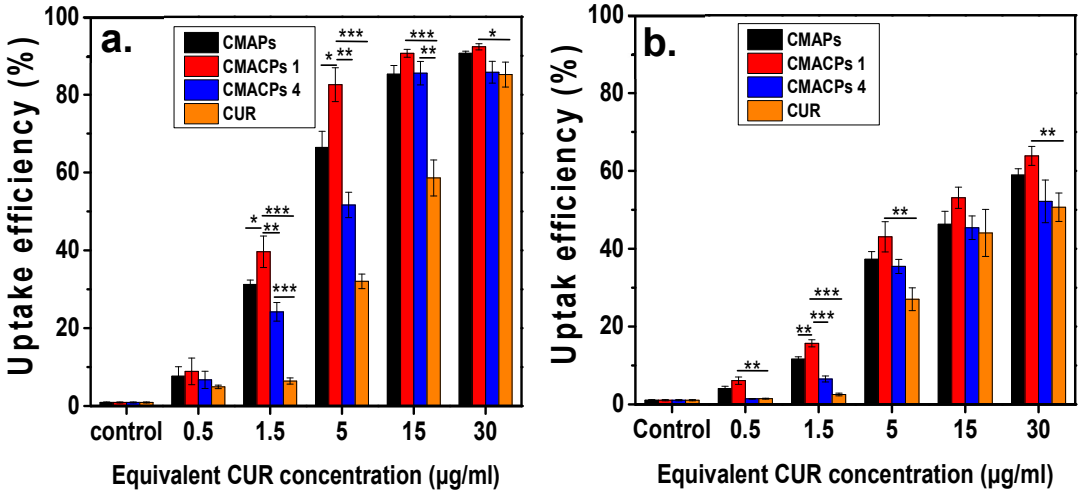

Fig. 6. Cellular uptake analysis of CUR in MDA-MB-231 cells (a) and HDF cells (b) after incubation with CMAPs, CMACPs 1 & 4 and free CUR for 24 h. The CUR uptake was analysed by flow cytometry. The dosages of CUR in particles were equivalent to the amounts of free CUR used. CMACPs 1 & 4 represent CMACPs that possess 1 & 4 layers of

Peer-reviewed version available at Nanomaterials 2018, 8, 907; doi:10.3390/nano8110907

polymers coated on MNPs respectively. The results are shown in mean ± SD, n = 3. The statistical significance is expressed as *** $p < 0.001$, ** $p < 0.01$, * $p < 0.05$.

To investigate the cellular uptake kinetics of CMAPs and CMACPs, MDA-MB-231 breast cancer cells and HDF cells were incubated with free CUR and particles containing equivalent amount of CUR for 24 h. The resultant cells were analysed by flow cytometry to determine the cellular uptake of CUR by different cells. As shown in Fig. 6a, it is evident that the percentage of MDA-MB-231 cells that have taken up CUR was CUR dose dependant. Significant higher uptake efficiency was observed for MDA-MB-231 cells treated with CMAPs and CMACPs than those treated with free CUR, indicating that the nanoparticles increase the CUR uptake. This is in agreement with previously reported data[1,31,74-76] that CUR uptake through nano formulations is at least 2-3 fold greater than free CUR [1]. Here, at a CUR concentration of 1.5 μg/ml, an uptake efficiency of 31.2%, 39.6% and 24.2% was observed for MDA-MB-231 cells treated with CMAPs, CMACPs 1 & 4 respectively, which is 3-6 folds higher than the uptake efficiency of cells treated with free CUR. The increased CUR uptake of CMAPs was attributed to the fact that the CUR loaded nanoparticles were more easily taken up by cells via endocytosis due to their smaller size (172-199 nm), while highly hydrophobic CUR was insoluble in aqueous solutions forming larger aggregates, which are more difficult to be internalized by cells [75,77]. The order of uptake efficiency of free CUR and CUR loaded particles was CMACPs 1 > CMAPs >CMACPs 4 > free CUR. Particles with CHI outermost layer exhibited the highest uptake efficiency (39.6 %). This result is in agreement with work by Zhou *et al.*,[44] who compared the uptake efficiency of CHI / alginate coated poly (lactide-co-glycolide) nanoparticles and observed the uptake efficiency of particles with CHI outermost layer was higher than those having alginate as the outermost layer. The promoted CUR uptake by the CHI surface is because of the protonated amino groups, which tended to interact with the negatively charged cell surfaces and promote the accumulation of CMACPs 1 onto the surface of MDA-MB-231 cells. Fig. 6b shows the CUR uptake efficiency for HDF cells after being treated with free CUR and CUR loaded particles. HDF cells exhibited a similar uptake pattern but an overall much lower CUR uptake efficiency compared to MDA-MB-231 cells, suggesting

Peer-reviewed version available at Nanomaterials 2018, 8, 907; doi:10.3390/nano8110907

CMAPs and CMACPs tended to target cancer cells rather than normal cells. This is in agreement with many previously reports that the cancer cells normally exhibit higher uptake efficiencies of CUR and CUR loaded nanoparticles than normal cells [29,78-80]. Cancer cells possess a higher metabolic activity to normal cells and their surface tends to overexpress various receptors which increase the available binding sites and therefore in turn promote a higher uptake efficiency of particles and drugs [81-83].

3.3.2. Magnetically targeted delivery assay

To investigate the potential of CMAPs and CMACPs for magnetically targeted delivery of CUR, free CUR, CMAPs and CMACPs were incubated with MDA-MB-231 cells in glass bottom dishes. A Neodymium magnet was placed under certain area of the dish to allow for the accumulation of magnetic nanoparticles within that area. Taking advantage of the auto-fluorescent property of CUR, the confocal fluorescence images show the cellular uptake of CUR in and out of the magnet-affected areas. The overall fluorescent intensity of MDA-MB-231 cells within the magnet-affected area that treated with free CUR (Fig. 7a) was obviously lower compared to cells treated with CUR loaded nanoparticles (Fig. 7c, e&g), suggesting CMAPs and CMACPs have enhanced the uptake of CUR. This result is consistent with the uptake efficiency shown in Fig. 6. No obvious difference on fluorescent intensities was observed between Fig. 7a and b, showing that the free CUR uptake is not affected by the presence of magnetic forces.

In contrast, cells treated with CMAPs (Fig. 7c), CMACPs 1 (Fig. 7e) and CMACPs 4 (Fig. 7g) within the magnet-affected area showed a profound increase fluorescent intensity compared to the cells treated with same particles but outside of the magnet-affected areas (Fig. 7d, f & h). The enhanced CUR uptake in the magnetic-affected areas was attributed to the accumulation of CUR loaded magnetic nanoparticles to the specified areas driven by the magnetic force. On the other hand, the local concentration of CUR loaded magnetic particles outside the magnet-affected areas was significantly lower, thus showing much lower fluorescent intensities. This result clearly shows that CMAPs and CMACPs have the potential for targeted drug delivery.

Peer-reviewed version available at Nanomaterials 2018, 8, 907; doi:10.3390/nano8110907

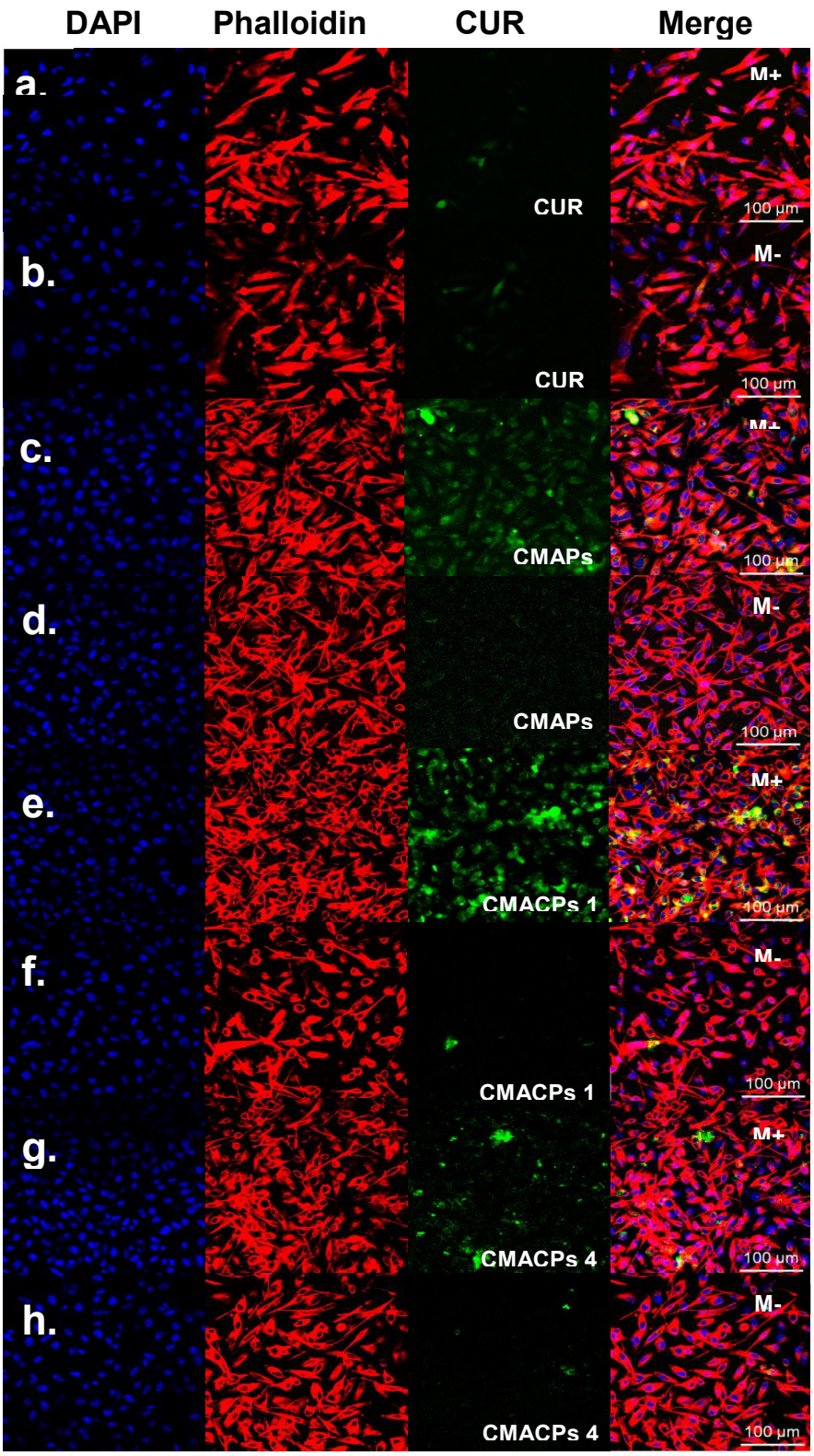

Fig. 7. Confocal fluorescence microscopy images of MDA-MB-231 cells incubated with free CUR (a & b), CMAPs (c & d), CMACPs 1 (e & f) and CMACPs 4 (g & h). CMACPs 1 & 4 represent CMACPs that possess 1 & 4 layers of polymers coated on MNPs respectively. CUR

loaded particles contained equivalent amount of drug as free CUR (5 μg/ml). Cell nucleus and cytoskeleton were stained with DAPI (blue) and Alexa Fluor 568 Phalloidin (red). M+ denotes the images taken within the magnet affected area and M- denotes the images taken outside of the magnet-affected area.

3.4. *In vitro* cytotoxicity assay

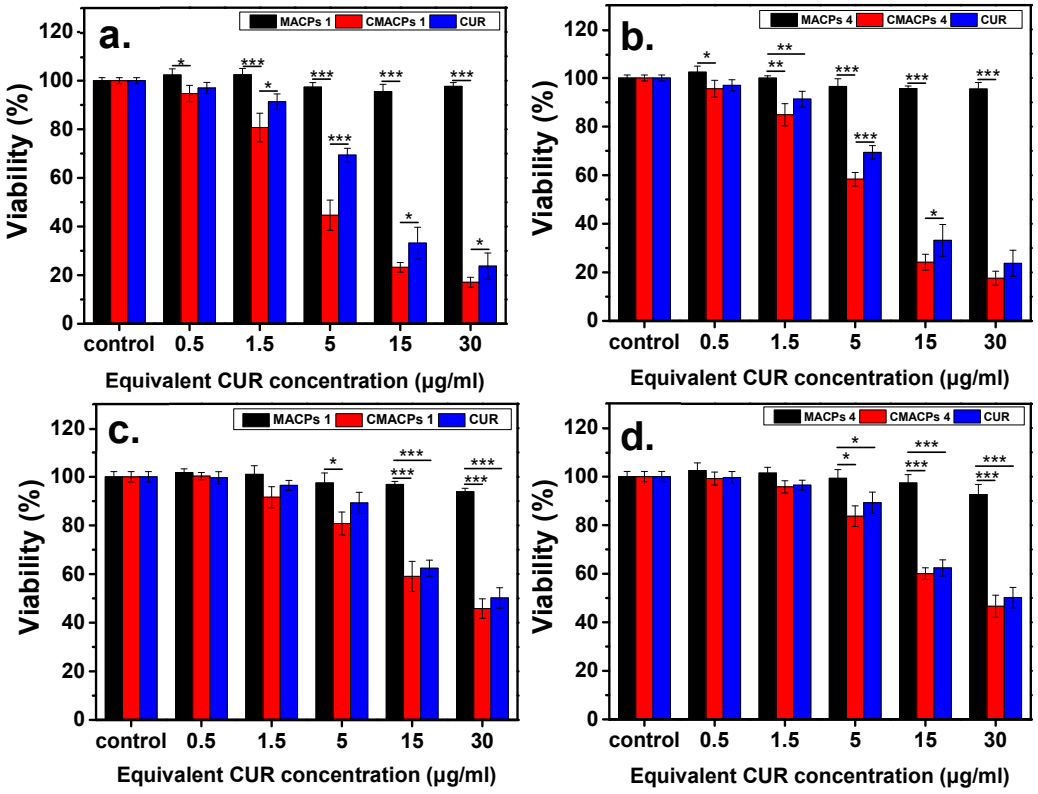

Fig. 8. The *in vitro* MTT assay suggested CMACPs exhibited significantly higher cytotoxicity toward MDA-MB-231 breast cancer cells than to HDF cells. MDA-MB-231 cells (a & b) and HDF cells (c & d) were treated with free CUR, CMACPs 1, CMACPs 4 and blank MACPs 1, MACPs 4 for 48 h. CMACPs 1 & 4 (or MACPs 1 & 4) represent CMACPs (or MACPs) that possess 1 & 4 layers of polymers, respectively. The amounts of CUR in CUR loaded nanoparticles were equivalent to the amounts of free CUR (0.5-30 μg/ml), respectively. The results are shown in mean ± SD, n ≥ 3. The statistical significance is expressed as *** $p < 0.001$, ** $p < 0.01$, * $p < 0.05$.

Peer-reviewed version available at Nanomaterials 2018, 8, 907; doi:10.3390/nano8110907

In order to investigate the cytotoxicity of CMACPs toward cancer and normal cells, MDA-MB-231 breast cancer cells and HDF cells were incubated with free CUR, CMACPs 1, CMACPs 4 and blank MACPs for 48 h. The in vitro MTT assay results are shown in Fig. 8. It can be observed in Fig. 8a & b that both free CUR and CMACPs exhibited increased cytotoxicity toward MDA-MB-231 cells with increasing CUR concentration, which was in agreement with previously reported data that CUR possessed dose dependent cytotoxicity towards cancer cells [1,31,74-76]. Both CMACPs 1 and 4 showed enhanced cytotoxicity toward MDA-MB-231 cells compared to free CUR, which was attributed to the enhanced uptake of CMACPs. As discussed in section 3.4.1, the uptake efficiency of MDA-MB-231 cells treated with CMACPs was 3-6 fold greater than those treated with free CUR. It is expected that the sustained release of CUR from internalized CMACPs maintained a high CUR concentration within the MDA-MB-231 cells, thus leading to lower viability of cells. CMACPs 1 were observed to exhibit higher cytotoxicity toward MDA-MB-231 cells than CMACPs 4, which was due to their higher CUR release rate (Fig. 5c) and uptake efficiency (Fig. 6a). As shown in Fig. 8c & d, the viability of HDF cells after treatment with free CUR and CMACPs was reduced at higher CUR concentrations (> 15 μg/ml) but significantly less affected at CUR concentrations less than 15 μg/ml compared to MDA-MB-231 cancer cells. This is in agreement with many previously studies, indicating CUR shows specific cytotoxicity towards cancer cells [29,78-80]. One of the major accepted theories is that cancer cells possess lower glutathione levels than normal cells due to their reprogrammed metabolic pathways [30]. Depletion of glutathione, which is important for the sensitivity of cells to CUR can lead to the enhancement of CUR sensitivity of cancer cells [30,78,84]. In addition, most cancer cells, but not normal cells, express constitutively active NF-KB that mediates their survival. CUR can suppress NF-KB regulated gene products, thus suppressing the proliferation of cancer cells [78,85]. Higher viabilities were observed for both MDA-MB-231 cells and HDF cells after they were treated with blank MACPs, demonstrating that MACPs are non-toxic toward these cells.

Peer-reviewed version available at Nanomaterials 2018, 8, 907; doi:10.3390/nano8110907

4. Conclusions

MACPs were prepared by a layer-by-layer coating of CHI and SA onto the surface of Fe_3O_4 nanoparticles. The successful coating of CHI and SA was confirmed by the zeta potential and FTIR spectra measurements of the particles. Incorporation of CUR was confirmed by the change of surface charge and morphology of CMACPs, while the mean diameter of CMACPs was lower than 200 nm and within the optimum size range for drug delivery applications. *In vitro* drug release profiles illustrated the sustained release of CUR from CMACPs and indicated that it was possible to control the release rate by altering the outermost polymer (CHI or SA) as well as by changing the number of polymer layers. More polymer layers resulted in a slower CUR drug release, where CHI as the outermost layer showed a faster CUR release than SA. Confocal fluorescence microscopic images confirmed the successful internalization of CUR into MDA-MB-231 breast cancer cells and indicated that rapid and targeted delivery of CUR can be achieved in the presence of an external magnetic field. FACS analysis indicated the CMACPs mediated uptake of CUR by MDA-MB-231 cells was 3-6 fold greater than that of free CUR. MDA-MB-231 cancer cells showed a significantly higher uptake efficiency of CUR than that of HDF normal cells after being treated with CMACPs. The MTT assay indicated that CMACPs exhibited a significantly higher cytotoxicity toward MDA-MB-231 cancer cells than toward HDF cells. In summary, the sustained release profiles, enhanced uptake efficiency and strong cytotoxicity to cancer cells as well as the potential for targeted delivery make MACPs a promising candidate for anti-cancer drug delivery.

Author Contributions: Conceptualization, X. Zhao and W. Song; Methodology, experiments and data analysis, W Song, X. Su, and W. Li; manuscript Preparation, W. Song, Z. Cai, and X. Zhao. All authors read and approved the manuscript.

Funding: The authors would like to thank EPSRC (EP/N007174/1 and EP/N023579/1), Royal Society (RG160662) and Jiangsu specially-appointed professors program for support.

Conflicts of Interest: The authors declare no conflicts of interest.

References

1. M Yallapu, M.; Jaggi, M.; C Chauhan, S. Curcumin nanomedicine: a road to cancer therapeutics. *Curr Pharm Des* **2013**, *19*, 1994-2010, doi:10.2174/138161213805289219.
2. Chattopadhyay, I.; Biswas, K.; Bandyopadhyay, U.; Banerjee, R.K. Turmeric and curcumin: Biological actions and medicinal applications. *Curr. Sci.(Bangalore)* **2004**, *87*, 44-53.
3. Masuda, T.; Hidaka, K.; Shinohara, A.; Maekawa, T.; Takeda, Y.; Yamaguchi, H. Chemical studies on antioxidant mechanism of curcuminoid: analysis of radical reaction products from curcumin and Linoleate. *J. Agric. Food Chem.* **1999**, *47*, 71-77, doi: 10.1021/jf9805348.
4. Ruby, A.; Kuttan, G.; Babu, K.D.; Rajasekharan, K.; Kuttan, R. Anti-tumour and antioxidant activity of natural curcuminoids. *Cancer Lett.* **1995**, *94*, 79-83, doi:10.1016/0304-3835(95)03827-J.
5. Ak, T.; Gulcin, I. Antioxidant and radical scavenging properties of curcumin. *Chem Biol Interact* **2008**, *174*, 27-37, doi:10.1016/j.cbi.2008.05.003.
6. Brouet, I.; Ohshima, H. Curcumin, an anti-tumor promoter and anti-inflammatory agent, inhibits induction of nitric oxide synthase in activated macrophages. *Biochem. Biophys. Res. Commun.* **1995**, *206*, 533-540, doi:10.1006/bbrc.1995.1076.
7. Kawamori, T.; Lubet, R.; Steele, V.E.; Kelloff, G.J.; Kaskey, R.B.; Rao, C.V.; Reddy, B.S. Chemopreventive effect of curcumin, a naturally occurring anti-inflammatory agent, during the promotion/progression stages of colon cancer. *Cancer Res.* **1999**, *59*, 597-601.
8. Aggarwal, B.B.; Harikumar, K.B. Potential therapeutic effects of curcumin, the anti-inflammatory agent, against neurodegenerative, cardiovascular, pulmonary, metabolic, autoimmune and neoplastic diseases. *Int J Biochem Cell Biol* **2009**, *41*, 40-59, doi:10.1016/j.biocel.2008.06.010.
9. Sidhu, G.S.; Singh, A.K.; Thaloor, D.; Banaudha, K.K.; Patnaik, G.K.; Srimal, R.C.; Maheshwari, R.K. Enhancement of wound healing by curcumin in animals. *Wound Repair Regen.* **1998**, *6*, 167-177, doi:10.1046/j.1524-475X.1998.60211.x.
10. Panchatcharam, M.; Miriyala, S.; Gayathri, V.S.; Suguna, L. Curcumin improves wound healing by modulating collagen and decreasing reactive oxygen species. *Mol Cell Biochem* **2006**, *290*, 87-96, doi:10.1007/s11010-006-9170-2.
11. Negi, P.; Jayaprakasha, G.; Jagan Mohan Rao, L.; Sakariah, K. Antibacterial activity of turmeric oil: a byproduct from curcumin manufacture. *J. Agric. Food Chem.* **1999**, *47*, 4297-4300, doi:10.1021/jf990308d.
12. Mun, S.H.; Joung, D.K.; Kim, Y.S.; Kang, O.H.; Kim, S.B.; Seo, Y.S.; Kim, Y.C.; Lee, D.S.; Shin, D.W.; Kweon, K.T., et al. Synergistic antibacterial effect of curcumin against methicillin-resistant Staphylococcus aureus. *Phytomedicine* **2013**, *20*, 714-718, doi:10.1016/j.phymed.2013.02.006.
13. Rezaee, R.; Momtazi, A.A.; Monemi, A.; Sahebkar, A. Curcumin: a potentially powerful tool to reverse cisplatin-induced toxicity. *Pharmacol. Res* **2016**, *117*, 218-227, doi: 10.1016/j.phrs.2016.12.037.

14. Wilken, R.; Veena, M.S.; Wang, M.B.; Srivatsan, E.S. Curcumin: A review of anti-cancer properties and therapeutic activity in head and neck squamous cell carcinoma. *Mol Cancer* **2011**, *10*, 12, doi:10.1186/1476-4598-10-12.
15. Aggarwal, B.B.; Kumar, A.; Bharti, A.C. Anticancer potential of curcumin: preclinical and clinical studies. *Anticancer res* **2003**, *23*, 363-398.
16. Li, M.; Zhang, Z.; Hill, D.L.; Wang, H.; Zhang, R. Curcumin, a dietary component, has anticancer, chemosensitization, and radiosensitization effects by down-regulating the MDM2 oncogene through the PI3K/mTOR/ETS2 pathway. *Cancer Res* **2007**, *67*, 1988-1996, doi:10.1158/0008-5472.CAN-06-3066.
17. Tapal, A.; Tiku, P.K. Complexation of curcumin with soy protein isolate and its implications on solubility and stability of curcumin. *Food Chem.* **2012**, *130*, 960-965, doi:10.1016/j.foodchem.2011.08.025.
18. Wan, S.; Sun, Y.; Qi, X.; Tan, F. Improved bioavailability of poorly water-soluble drug curcumin in cellulose acetate solid dispersion. *AAPS PharmSciTech* **2012**, *13*, 159-166, doi:10.1208/s12249-011-9732-9.
19. Sahu, A.; Bora, U.; Kasoju, N.; Goswami, P. Synthesis of novel biodegradable and self-assembling methoxy poly (ethylene glycol)–palmitate nanocarrier for curcumin delivery to cancer cells. *Acta Biomater* **2008**, *4*, 1752-1761, doi:10.1016/j.actbio.2008.04.021.
20. Shoba, G.; Joy, D.; Joseph, T.; Majeed, M.; Rajendran, R.; Srinivas, P. Influence of piperine on the pharmacokinetics of curcumin in animals and human volunteers. *Planta Med.* **1998**, *64*, 353-356, doi:10.1055/s-2006-957450.
21. Liu, A.; Lou, H.; Zhao, L.; Fan, P. Validated LC/MS/MS assay for curcumin and tetrahydrocurcumin in rat plasma and application to pharmacokinetic study of phospholipid complex of curcumin. *J Pharm Biomed Anal* **2006**, *40*, 720-727, doi:10.1016/j.jpba.2005.09.032.
22. Tiyaboonchai, W.; Tungpradit, W.; Plianbangchang, P. Formulation and characterization of curcuminoids loaded solid lipid nanoparticles. *Int J Pharm* **2007**, *337*, 299-306, doi:10.1016/j.ijpharm.2006.12.043.
23. Li, L.; Braiteh, F.S.; Kurzrock, R. Liposome-encapsulated curcumin: in vitro and in vivo effects on proliferation, apoptosis, signaling, and angiogenesis. *J. Clin. Oncol.* **2005**, *104*, 1322-1331, doi:10.1002/cncr.21300.
24. Hajj Ali, H.; Michaux, F.; Ntsama, B.; Sandrine, I.; Durand, P.; Jasniewski, J.; Linder, M. Shea butter solid nanoparticles for curcumin encapsulation: Influence of nanoparticles size on drug loading. *Eur J Lipid Sci Technol* **2016**, *118*, 1168-1178, doi:10.1002/ejlt.201500348
25. Wang, T.; Ma, X.; Lei, Y.; Luo, Y. Solid lipid nanoparticles coated with cross-linked polymeric double layer for oral delivery of curcumin. *Colloids Surf B Biointerfaces* **2016**, *148*, 1-11, doi:10.1016/j.colsurfb.2016.08.047.
26. Zhang, J.; Tang, Q.; Xu, X.; Li, N. Development and evaluation of a novel phytosome-loaded chitosan microsphere system for curcumin delivery. *Int. J. Pharm.* **2013**, *448*, 168-174, doi:10.1016/j.ijpharm.2013.03.021.

27. Xie, M.-B.; Li, Y.; Zhao, Z.; Chen, A.-Z.; Li, J.-S.; Hu, J.-Y.; Li, G.; Li, Z. Solubility enhancement of curcumin via supercritical CO 2 based silk fibroin carrier. *J. Supercrit. Fluids* **2015**, *103*, 1-9, doi:10.1016/j.supflu.2015.04.021.
28. Song, W.; Muthana, M.; Mukherjee, J.; Falconer, R.J.; Biggs, C.A.; Zhao, X. Magnetic-Silk Core-Shell Nanoparticles as Potential Carriers for Targeted Delivery of Curcumin into Human Breast Cancer Cells. *ACS Biomater Sci Eng* **2017**, *3*, 1027-1038, doi:10.1021/acsbiomaterials.7b00153.
29. Anitha, A.; Maya, S.; Deepa, N.; Chennazhi, K.; Nair, S.; Tamura, H.; Jayakumar, R. Efficient water soluble O-carboxymethyl chitosan nanocarrier for the delivery of curcumin to cancer cells. *Carbohydr. Polym.* **2011**, *83*, 452-461, doi:10.1016/j.carbpol.2010.08.008.
30. Montalbán, M.G.; Coburn, J.M.; Lozano-Pérez, A.A.; Cenis, J.L.; Víllora, G.; Kaplan, D.L. Production of curcumin-loaded silk fibroin nanoparticles for cancer therapy. *Nanomaterials* **2018**, *8*, 126, doi:10.3390/nano8020126.
31. Liu, J.; Xu, L.; Liu, C.; Zhang, D.; Wang, S.; Deng, Z.; Lou, W.; Xu, H.; Bai, Q.; Ma, J. Preparation and characterization of cationic curcumin nanoparticles for improvement of cellular uptake. *Carbohydr. Polym.* **2012**, *90*, 16-22, doi:10.1016/j.carbpol.2012.04.036.
32. Chuah, L.H.; Billa, N.; Roberts, C.J.; Burley, J.C.; Manickam, S. Curcumin-containing chitosan nanoparticles as a potential mucoadhesive delivery system to the colon. *Pharm Dev Technol* **2013**, *18*, 591-599, doi:10.3109/10837450.2011.640688.
33. Bhandari, R.; Gupta, P.; Dziubla, T.; Hilt, J.Z. Single step synthesis, characterization and applications of curcumin functionalized iron oxide magnetic nanoparticles. *Mater Sci Eng C* **2016**, *67*, 59-64, doi:10.1016/j.msec.2016.04.093.
34. Lee, K.Y.; Mooney, D.J. Alginate: properties and biomedical applications. *Prog. Polym. Sci.* **2012**, *37*, 106-126, doi:10.1016/j.progpolymsci.2011.06.003.
35. Bhunchu, S.; Rojsitthisak, P. Biopolymeric alginate-chitosan nanoparticles as drug delivery carriers for cancer therapy. *Pharmazie* **2014**, *69*, 563-570, doi:10.1691/ph.2014.3165.
36. Agnihotri, S.A.; Mallikarjuna, N.N.; Aminabhavi, T.M. Recent advances on chitosan-based micro-and nanoparticles in drug delivery. *J Control Release.* **2004**, *100*, 5-28, doi:10.1016/j.jconrel.2004.08.010.
37. Ching, S.H.; Bansal, N.; Bhandari, B. Alginate gel particles–A review of production techniques and physical properties. *Crit Rev Food Sci Nutr* **2017**, *57*, 1133-1152, doi:10.1080/10408398.2014.965773.
38. Rampino, A.; Borgogna, M.; Blasi, P.; Bellich, B.; Cesàro, A. Chitosan nanoparticles: preparation, size evolution and stability. *Int. J. Pharm.* **2013**, *455*, 219-228, doi:10.1016/j.ijpharm.2013.07.034.
39. Bernkop-Schnürch, A.; Dünnhaupt, S. Chitosan-based drug delivery systems. *Eur J Pharm Biopharm* **2012**, *81*, 463-469, doi:10.1016/j.ejpb.2012.04.007.
40. Anitha, A.; Deepagan, V.; Rani, V.D.; Menon, D.; Nair, S.; Jayakumar, R. Preparation, characterization, in vitro drug release and biological studies of

curcumin loaded dextran sulphate–chitosan nanoparticles. *Carbohydr. Polym.* **2011**, *84*, 1158-1164, doi:10.1016/j.carbpol.2011.01.005.

41. Ahmadi, F.; Ghasemi-Kasman, M.; Ghasemi, S.; Tabari, M.G.; Pourbagher, R.; Kazemi, S.; Alinejad-Mir, A. Induction of apoptosis in hela cancer cells by an ultrasonic-mediated synthesis of curcumin-loaded chitosan–alginate–sTPP nanoparticles. *Int. J. Nanomed.* **2017**, *12*, 8545-8556, doi:10.2147/IJN.S146516.
42. Maghsoudi, A.; Yazdian, F.; Shahmoradi, S.; Ghaderi, L.; Hemati, M.; Amoabediny, G. Curcumin-loaded polysaccharide nanoparticles: optimization and anticariogenic activity against Streptococcus mutans. *Mater Sci Eng C* **2017**, *75*, 1259-1267, doi:10.1016/j.msec.2017.03.032.
43. Martins, A.F.; Bueno, P.V.; Almeida, E.A.; Rodrigues, F.H.; Rubira, A.F.; Muniz, E.C. Characterization of N-trimethyl chitosan/alginate complexes and curcumin release. *Int J Biol Macromol* **2013**, *57*, 174-184, doi:10.1016/j.ijbiomac.2013.03.029.
44. Zhou, J.; Romero, G.; Rojas, E.; Ma, L.; Moya, S.; Gao, C. Layer by layer chitosan/alginate coatings on poly (lactide-co-glycolide) nanoparticles for antifouling protection and Folic acid binding to achieve selective cell targeting. *J Colloid Interface Sci* **2010**, *345*, 241-247, doi:10.1016/j.jcis.2010.02.004.
45. Chai, F.; Sun, L.; He, X.; Li, J.; Liu, Y.; Xiong, F.; Ge, L.; Webster, T.J.; Zheng, C. Doxorubicin-loaded poly (lactic-co-glycolic acid) nanoparticles coated with chitosan/alginate by layer by layer technology for antitumor applications. *Int. J. Nanomed.* **2017**, *12*, 1791, doi:10.2147/IJN.S130404.
46. Haidar, Z.S.; Hamdy, R.C.; Tabrizian, M. Protein release kinetics for core–shell hybrid nanoparticles based on the layer-by-layer assembly of alginate and chitosan on liposomes. *Biomaterials* **2008**, *29*, 1207-1215, doi:10.1016/j.biomaterials.2007.11.012.
47. Zhou, J.; Moya, S.; Ma, L.; Gao, C.; Shen, J. Polyelectrolyte coated PLGA nanoparticles: templation and release behavior. *Macromol Biosci* **2009**, *9*, 326-335, doi:10.1002/mabi.200800188
48. Wang, Z.; Zhang, X.; Gu, J.; Yang, H.; Nie, J.; Ma, G. Electrodeposition of alginate/chitosan layer-by-layer composite coatings on titanium substrates. *Carbohydr. Polym.* **2014**, *103*, 38-45, doi:10.1016/j.carbpol.2013.12.007.
49. Zhou, G.; Lu, Y.; Zhang, H.; Chen, Y.; Yu, Y.; Gao, J.; Sun, D.; Zhang, G.; Zou, H.; Zhong, Y. A novel pulsed drug-delivery system: polyelectrolyte layer-by-layer coating of chitosan–alginate microgels. *Int. J. Nanomed.* **2013**, *8*, 877-887, doi:10.2147/IJN.S38144.
50. Arruebo, M.; Fernández-Pacheco, R.; Ibarra, M.R.; Santamaría, J. Magnetic nanoparticles for drug delivery. *Nano today* **2007**, *2*, 22-32, doi:10.1016/S1748-0132(07)70084-1.
51. Iannone, A.; Magin, R.; Walczak, T.; Federico, M.; Swartz, H.; Tomasi, A.; Vannini, V. Blood clearance of dextran magnetite particles determined by a noninvasive in vivo ESR method. *Magn Reson Med* **1991**, *22*, 435-442, doi:10.1002/mrm.1910220251.

52. Liu, X.; Chen, X.; Li, Y.; Wang, X.; Peng, X.; Zhu, W. Preparation of superparamagnetic Fe3O4@ alginate/chitosan nanospheres for Candida rugosa lipase immobilization and utilization of layer-by-layer assembly to enhance the stability of immobilized lipase. *ACS Appl. Mater. Interfaces* **2012**, *4*, 5169-5178, doi:10.1021/am301104c.
53. Ching, S.H.; Bhandari, B.; Webb, R.; Bansal, N. Visualizing the interaction between sodium caseinate and calcium alginate microgel particles. *Food Hydrocoll* **2015**, *43*, 165-171, doi:10.1016/j.foodhyd.2014.05.013.
54. dos Santos Silva, M.; Cocenza, D.S.; Grillo, R.; de Melo, N.F.S.; Tonello, P.S.; de Oliveira, L.C.; Cassimiro, D.L.; Rosa, A.H.; Fraceto, L.F. Paraquat-loaded alginate/chitosan nanoparticles: preparation, characterization and soil sorption studies. *J Hazard Mater* **2011**, *190*, 366-374, doi:10.1016/j.jhazmat.2011.03.057.
55. Maldonado, L., and J. Kokini. An optimal window for the fabrication of Edible Polyelectrolyte Complex Nanotubes (EPCNs) from bovine serum albumin (BSA) and sodium alginate. *Food Hydrocoll* **2017**, 10.1016/j.foodhyd.2017.10.010, doi:10.1016/j.foodhyd.2017.10.010.
56. Donati, I.; Paoletti, S. Material properties of alginates. In *Alginates: Biology and applications*, Springer: 2009; pp. 1-53.
57. Swain, S.; Dey, R.; Islam, M.; Patel, R.; Jha, U.; Patnaik, T.; Airoldi, C. Removal of fluoride from aqueous solution using aluminum-impregnated chitosan biopolymer. *Sep. Sci.* **2009**, *44*, 2096-2116, doi:10.1080/01496390902881212.
58. Acevedo-Fani, A.; Salvia-Trujillo, L.; Soliva-Fortuny, R.; Martín-Belloso, O. Layer-by-Layer Assembly of Food-Grade Alginate/Chitosan Nanolaminates: Formation and Physicochemical Characterization. *Food Biophys* **2017**, *12*, 299-308, doi:10.1007/s11483-017-9486-3.
59. Rivera, M.C.; Pinheiro, A.C.; Bourbon, A.I.; Cerqueira, M.A.; Vicente, A.A. Hollow chitosan/alginate nanocapsules for bioactive compound delivery. *Int J Biol Macromol* **2015**, *79*, 95-102, doi:10.1016/j.ijbiomac.2015.03.003.
60. Wasan, K.M. *Role of lipid excipients in modifying oral and parenteral drug delivery: Basic principles and biological examples*; John Wiley & Sons: 2007.
61. Qiu, H.; Qiu, Z.; Wang, J.; Zhang, R.; Zheng, F. Enhanced swelling and methylene blue adsorption of polyacrylamide‐based superabsorbents using alginate modified montmorillonite. *J Appl Polym Sci* **2014**, *131*, doi:10.1002/app.40013
62. Kevadiya, B.D.; Joshi, G.V.; Patel, H.A.; Ingole, P.G.; Mody, H.M.; Bajaj, H.C. Montmorillonite-alginate nanocomposites as a drug delivery system: Intercalation and in vitro release of vitamin B1 and vitamin B6. *J Biomater Appl* **2010**, *25*, 161-177, doi:10.1177/0885328209344003.
63. Sartori, C.; Finch, D.S.; Ralph, B.; Gilding, K. Determination of the cation content of alginate thin films by FTi. r. spectroscopy. *Polymer* **1997**, *38*, 43-51, doi:10.1016/S0032-3861(96)00458-2.
64. Daemi, H.; Barikani, M. Synthesis and characterization of calcium alginate nanoparticles, sodium homopolymannuronate salt and its calcium nanoparticles. *Sci Iran* **2012**, *19*, 2023-2028, doi:10.1016/j.scient.2012.10.005.

65. Zeng, M.; Feng, Z.; Huang, Y.; Liu, J.; Ren, J.; Xu, Q.; Fan, L. Chemical structure and remarkably enhanced mechanical properties of chitosan-graft-poly (acrylic acid)/polyacrylamide double-network hydrogels. *Polym Bull* **2017**, *74*, 55-74, doi:10.1007/s00289-016-1697-0.
66. Su, X.; Mahalingam, S.; Edirisinghe, M.; Chen, B. Highly Stretchable and Highly Resilient Polymer–Clay Nanocomposite Hydrogels with Low Hysteresis. *ACS Appl. Mater. Interfaces* **2017**, *9*, 22223-22234, doi:10.1021/acsami.7b05261.
67. Liu, X.; Chen, X.; Li, Y.; Wang, X.; Peng, X.; Zhu, W. Preparation of Superparamagnetic Fe3O4@Alginate/Chitosan Nanospheres for Candida rugosa lipase Immobilization and Utilization of Layer-by-Layer Assembly to Enhance the Stability of Immobilized Lipase. *ACS Appl. Mater. Interfaces* **2012**, *4*, 5169-5178, doi:10.1021/am301104c.
68. Tiwari, S.; Mishra, B. Multilayered membrane-controlled microcapsules for controlled delivery of isoniazid. *Daru* **2011**, *19*, 41-46.
69. Aditya, N.; Aditya, S.; Yang, H.; Kim, H.W.; Park, S.O.; Ko, S. Co-delivery of hydrophobic curcumin and hydrophilic catechin by a water-in-oil-in-water double emulsion. *Food Chem.* **2015**, *173*, 7-13, doi:10.1016/j.foodchem.2014.09.131.
70. Altunbas, A.; Lee, S.J.; Rajasekaran, S.A.; Schneider, J.P.; Pochan, D.J. Encapsulation of curcumin in self-assembling peptide hydrogels as injectable drug delivery vehicles. *Biomaterials* **2011**, *32*, 5906-5914, doi:10.1016/j.biomaterials.2011.04.069.
71. Yang, F.; Lim, G.P.; Begum, A.N.; Ubeda, O.J.; Simmons, M.R.; Ambegaokar, S.S.; Chen, P.P.; Kayed, R.; Glabe, C.G.; Frautschy, S.A. Curcumin inhibits formation of amyloid β oligomers and fibrils, binds plaques, and reduces amyloid in vivo. *J Biol Chem* **2005**, *280*, 5892-5901, doi:10.1074/jbc.M404751200.
72. Manju, S.; Sreenivasan, K. Conjugation of curcumin onto hyaluronic acid enhances its aqueous solubility and stability. *J Colloid Interface Sci* **2011**, *359*, 318-325, doi:10.1016/j.jcis.2011.03.071.
73. Cui, J.; Yu, B.; Zhao, Y.; Zhu, W.; Li, H.; Lou, H.; Zhai, G. Enhancement of oral absorption of curcumin by self-microemulsifying drug delivery systems. *Int. J. Pharm.* **2009**, *371*, 148-155, doi:10.1016/j.ijpharm.2008.12.009.
74. Mohanty, C.; Acharya, S.; Mohanty, A.K.; Dilnawaz, F.; Sahoo, S.K. Curcumin-encapsulated MePEG/PCL diblock copolymeric micelles: a novel controlled delivery vehicle for cancer therapy. *Nanomedicine* **2010**, *5*, 433-449, doi:10.2217/nnm.10.9.
75. Zaman, M.S.; Chauhan, N.; Yallapu, M.M.; Gara, R.K.; Maher, D.M.; Kumari, S.; Sikander, M.; Khan, S.; Zafar, N.; Jaggi, M. Curcumin nanoformulation for cervical cancer treatment. *Sci Rep* **2016**, *6*, 20051, doi:10.1038/srep20051.
76. Mohan Yallapu, M.; Ray Dobberpuhl, M.; Michele Maher, D.; Jaggi, M.; Chand Chauhan, S. Design of curcumin loaded cellulose nanoparticles for prostate cancer. *Curr Drug Metab* **2012**, *13*, 120-128, doi:10.2174/138920012798356952.

77. Jagannathan, R.; Abraham, P.M.; Poddar, P. Temperature-dependent spectroscopic evidences of curcumin in aqueous medium: a mechanistic study of its solubility and stability. *J Phys Chem B* **2012**, *116*, 14533-14540, doi:10.1021/jp3050516.
78. Mangalathillam, S.; Rejinold, N.S.; Nair, A.; Lakshmanan, V.-K.; Nair, S.V.; Jayakumar, R. Curcumin loaded chitin nanogels for skin cancer treatment via the transdermal route. *Nanoscale* **2012**, *4*, 239-250, doi:10.1039/C1NR11271F.
79. Rejinold, N.S.; Sreerekha, P.; Chennazhi, K.; Nair, S.; Jayakumar, R. Biocompatible, biodegradable and thermo-sensitive chitosan-g-poly (N-isopropylacrylamide) nanocarrier for curcumin drug delivery. *Int J Biol Macromol* **2011**, *49*, 161-172, doi:10.1016/j.ijbiomac.2011.04.008.
80. Kunwar, A.; Barik, A.; Mishra, B.; Rathinasamy, K.; Pandey, R.; Priyadarsini, K. Quantitative cellular uptake, localization and cytotoxicity of curcumin in normal and tumor cells. *Biochim Biophys Acta Gen Subj* **2008**, *1780*, 673-679, doi:10.1016/j.bbagen.2007.11.016.
81. Chaves, N.L.; Estrela-Lopis, I.; Böttner, J.; Lopes, C.A.; Guido, B.C.; de Sousa, A.R.; Báo, S.N. Exploring cellular uptake of iron oxide nanoparticles associated with rhodium citrate in breast cancer cells. *Int. J. Nanomed.* **2017**, *12*, 5511-5523, doi:10.2147/IJN.S141582.
82. Kettler, K.; Veltman, K.; van de Meent, D.; van Wezel, A.; Hendriks, A.J. Cellular uptake of nanoparticles as determined by particle properties, experimental conditions, and cell type. *Environ Toxicol Chem* **2014**, *33*, 481-492, doi:10.1002/etc.2470.
83. Kohler, N.; Sun, C.; Wang, J.; Zhang, M. Methotrexate-modified superparamagnetic nanoparticles and their intracellular uptake into human cancer cells. *Langmuir* **2005**, *21*, 8858-8864, doi:10.1021/la0503451.
84. Syng-ai, C.; Kumari, A.L.; Khar, A. Effect of curcumin on normal and tumor cells: role of glutathione and bcl-2. *Mol Cancer Ther* **2004**, *3*, 1101-1108.
85. Shishodia, S.; Amin, H.M.; Lai, R.; Aggarwal, B.B. Curcumin (diferuloylmethane) inhibits constitutive NF-κB activation, induces G1/S arrest, suppresses proliferation, and induces apoptosis in mantle cell lymphoma. *Biochem Pharmacol* **2005**, *70*, 700-713, doi:10.1016/j.bcp.2005.04.043.